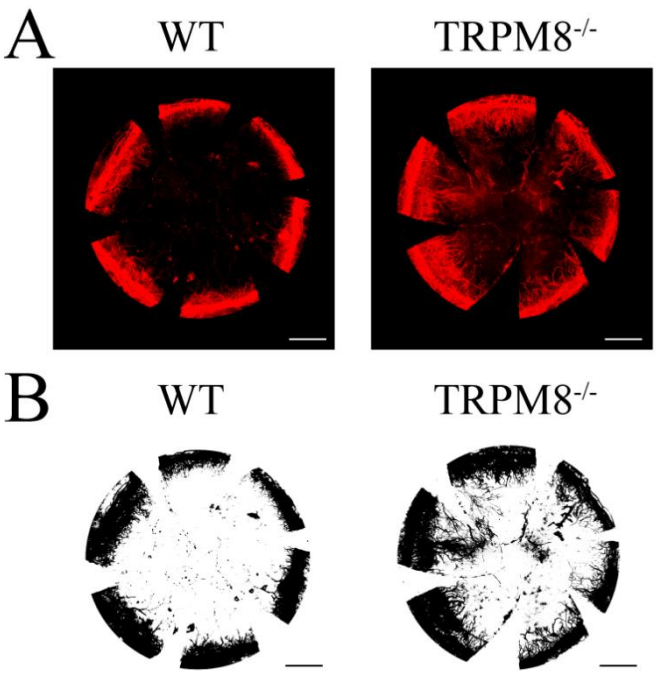

Figure S1. The CD31-staining blood vessels in corneal flat mounts staining in WT and TRPM8$^{-/-}$ mice 6 dpi. **(A)** showed the original view, and **(B)** showed grayscale image for analysis (scale bar = 500 μm).

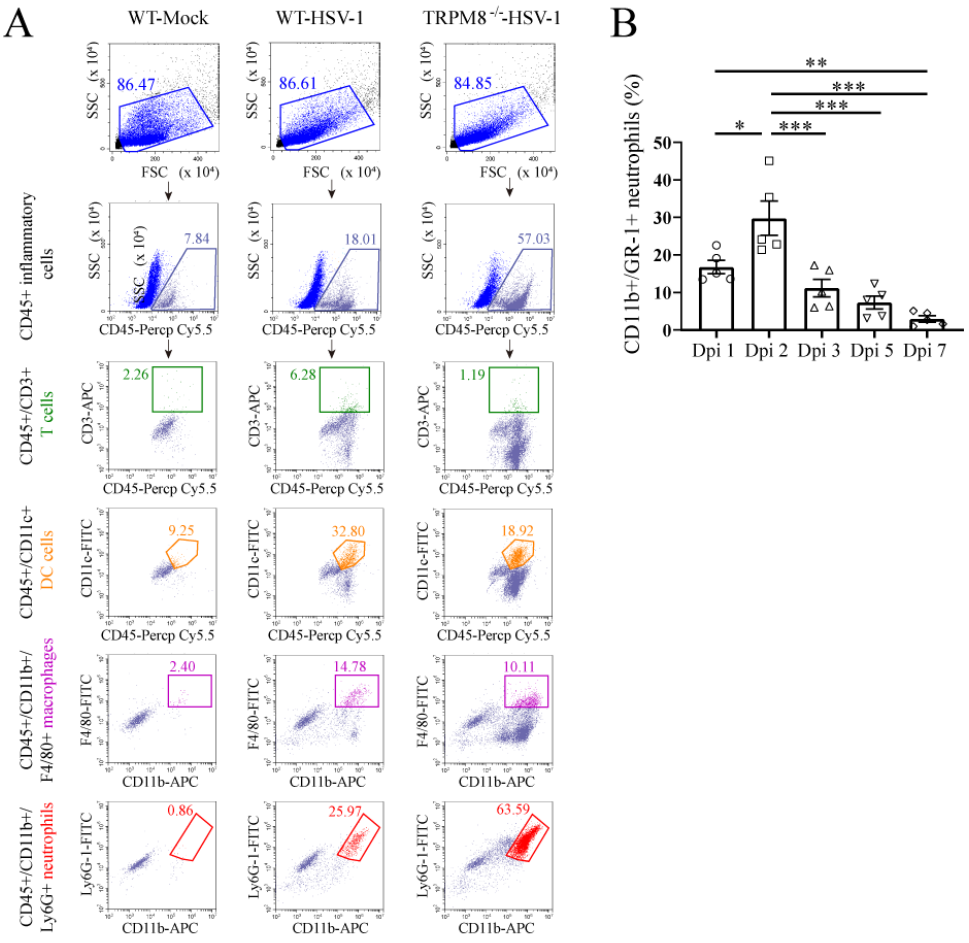

Figure S2. The leukocyte infiltration and dynamics of $CD11b^+$ $Ly6G^+$ cells infiltration during HSV-1 infection. **(A)** $TRPM8^{-/-}$ mice and WT mice were infected with culture medium (mock infection) or HSV-1 by corneal scarification. Immune responses in the cornea were analyzed 3 dpi by flow cytometry. FSC and SSC gating was used to exclude cell debris. Compared with WT mice, $TRPM8^{-/-}$ mice, if infected with HSV-1, had massive increased numbers of infiltrating $CD45^+$ $CD11b^+$ $Ly6G^+$ cells rather than $CD45^+$ $CD11b^+$ $F4/80^+$ macrophages, $CD45^+$ $CD3^+$ T cells and $CD45^+$ $CD11c^+$ DC cells. **(B)** Dynamics of $CD11b^+$ $Ly6G^+$ cells infiltration in WT mice. $CD11b^+$ $Ly6G^+$ cells migration into the cornea of WT mice began on 1 dpi, peaked at

2 dpi, and subsided slowly thereafter until 7 dpi (n = 5 per group). *p < 0.05, **p < 0.01, ***p < 0.001.

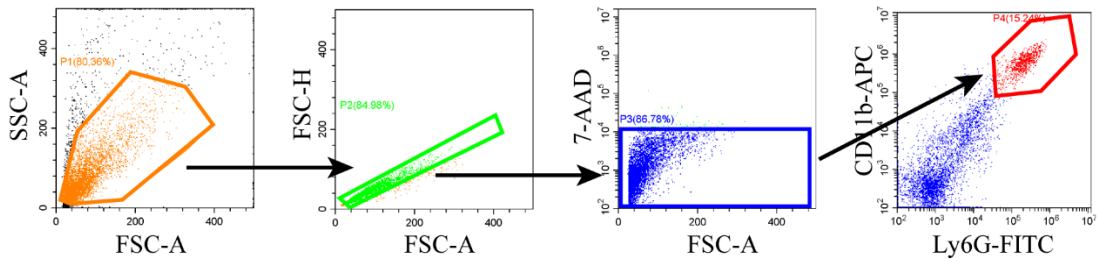

Figure S3. The new gating strategy used in flow cytometric analysis.

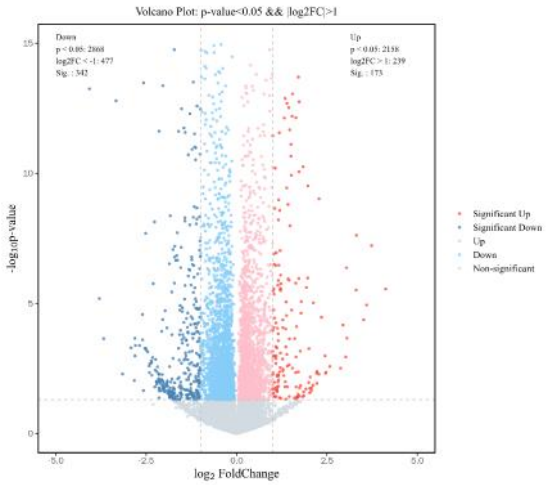

Figure S4. Volcano plot exhibiting differential expressed genes between WT mice and TRPM8$^{-/-}$ mice.

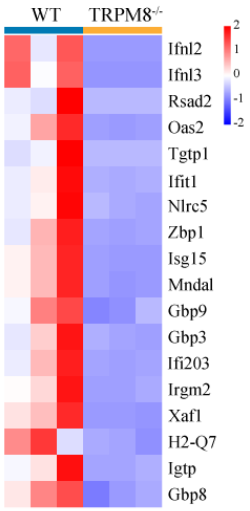

Figure S5. Heatmap showing the ISGs that were down-regulated in TRPM8$^{-/-}$ corneas compared with levels in WT corneas with no treatment.

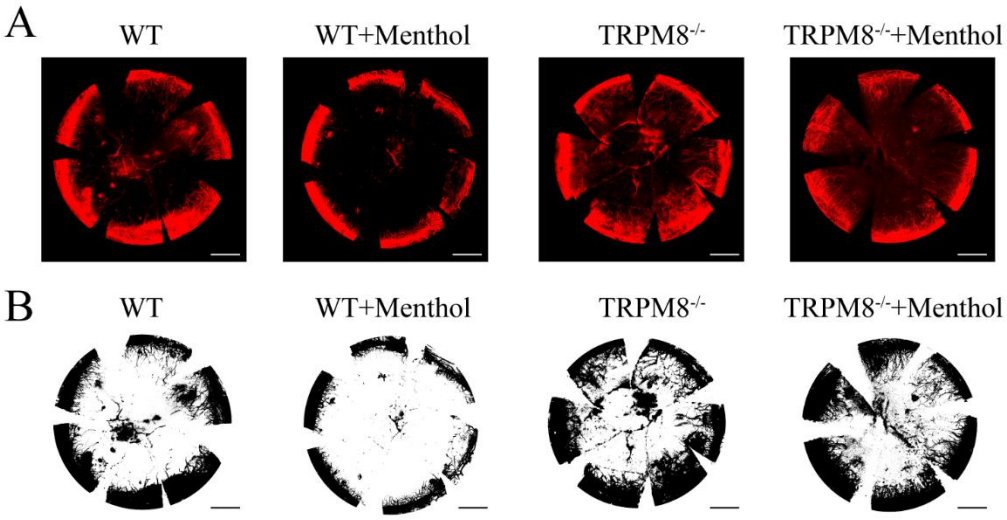

Figure S6. The CD31-staining blood vessels in corneal flat mounts staining in WT and TRPM8$^{-/-}$ mice with menthol or menthol control treatment 6 dpi. **(A)** showed the original view, and **(B)** showed grayscale image for analysis (scale bar = 500 μm).